Journal of Constructional Steel Research 66 (2010) 1248–1260

Contents lists available at ScienceDirect

Journal of Constructional Steel Research

journal homepage: www.elsevier.com/locate/jcsr

# Axial strength of circular concrete-filled steel tube columns — DOE approach

Manojkumar V. Chitawadagi [a,*], Mattur C. Narasimhan [a,1], S.M. Kulkarni [b,2]

[a] Department of Civil Engineering, National Institute of Technology, Karnataka, Surathkal, Mangalore-575025, India

[b] Department of Mechanical Engineering, National Institute of Technology Karnataka, Surathkal, Mangalore-575025, India

ARTICLE INFO

*Article history:*
Received 30 September 2009
Accepted 9 April 2010

*Keywords:*
Concrete-filled steel tubes
Columns
Circular tubes
Ultimate axial load
Axial shortening

ABSTRACT

This paper presents the effect of changes in diameter of the steel tube ($D$), wall thickness of the steel tube ($t$), strength of in-fill concrete ($f_{cu}$), and length of the tube ($L$) on ultimate axial load ($P_{ue}$) and axial shortening at the ultimate point ($\delta_{ue}$) of circular Concrete Filled steel Tubes (CFT). Taguchi's approach with an L9 orthogonal array is used to reduce the number of experiments. With the help of initial experiments, linear regression models are developed to predict the axial load and the axial shortening at the ultimate point. A total of 243 circular CFT samples are tested to verify the accuracy of these models at three factors with three levels. The experimental results are analyzed using Analysis Of Variance to investigate the most influencing factor on strength and axial shortening of CFT samples. Comparisons are made with predicted column strengths using the existing design codes, AISC-LRFD-2005 and EC4-1994.



## 1. Introduction

Concrete-Filled steel Tubular (CFT) columns have been increasingly used in many modern structures, such as dwelling houses, tall buildings, and arch bridges [1] The composite tubular columns have better structural performance than that of bare steel or reinforced concrete structural members. Steel hollow sections act as reinforcement for the concrete [2]. Steel–concrete composite members have advantageous qualities such as sufficient strength, ductility and stiffness. Generally, CFT columns have demonstrated a sufficient load capacity, ductility and energy absorption capacity. Concrete filled steel tubes are an economical column type, as the majority of the axial load is resisted by the concrete, which is less expensive than steel [3]. The steel tube serves as the formwork for casting the concrete, which reduces the construction cost. No other reinforcement is needed since the tube acts as longitudinal and lateral reinforcement for the concrete core.

The confining effect causes the core concrete to behave in a triaxial stress state while the core concrete prevents the wall of the steel hollow section from buckling inward. Experimental studies on concrete-filled steel tubes have been on-going for many decades. A review of available experimental studies shows that the main parameters affecting the behaviour and strength of concrete-filled columns are: the geometrical parameters, such as the slenderness, the diameter to wall thickness ($D/t$) ratio and the initial geometry of the column, and the mechanical parameters, such as the strength of the steel and concrete [4]. A primary deterrent to widespread use of CFTs is the limited knowledge regarding their behavior. A number of factors complicate the analysis and design of concrete-filled steel tubes [5]. Although CFT columns are suitable for tall buildings in high seismic regions, their use has been limited due to a lack of information about the true strength and inelastic behavior of CFT members [6]. Although the use of CFT columns is becoming more commonplace, concrete core confinement is not well understood [7].

The local buckling phenomenon was studied by many researchers. For axially loaded thin-walled steel tubes, local buckling of the steel tube does not occur if there is sufficient bond between the steel and concrete [8]. Based on the experimental results of 114 centrally loaded stub columns, Kenji Sakino et al. concluded that the difference between the ultimate strength and the nominal squash load of circular CFT columns, which are provided by confining the concrete, can be estimated as a linear function of the tube yield strength [9]. The improvement of the structural properties of CFT columns is mainly due to the composite action of the steel hollow section and the core concrete. The short-term composite action is such that the steel tube, in addition to acting as reinforcement, confines the concrete, resulting in a significant increase in concrete compressive strength, while the confined concrete not only relieves the steel tube of some load but also delays and moderates buckling deformations in the steel tube [10]. Eighty-one specimens were tested by Gupta et al. to investigate the effect of diameter and $D/t$ ratio of a steel tube on the load carrying capacity of the concrete filled tubular columns. The $D/t$ ratio was 25–39.

* Corresponding author. Tel.: +91 0824 247000 3041, Mobile: +91 9449837148.
*E-mail addresses:* manojkumar1966@gmail.com, mvc@bvb.edu, manojkumar1966@rediffmail.com (M.V. Chitawadagi), mattur_cn@yahoo.com (M.C. Narasimhan), samakoo@yahoo.com (S.M. Kulkarni).
[1] Tel.: +91 0824 247000x3041, Mobile: +91 9449163427.
[2] Tel.: +91 0824 247000x3656, Mobile: +91 9449086656.

0143-974X/$ – see front matter © 2010 Elsevier Ltd. All rights reserved.
doi:10.1016/j.jcsr.2010.04.006

**Nomenclature**

| | |
|---|---|
| $D$ | Outer diameter of the steel tube |
| $L$ | Length of the steel tube |
| $t$ | Wall thickness of the steel tube |
| $W$ | Water content |
| $f_{cu}$ | Cube compressive strength of concrete at 28 days |
| $P_{uc\text{-}G}$ | Generalized regression model to predict ultimate axial load |
| $P_{uc\text{-}N}$ | Predicted ultimate axial load based on initial nine experiments |
| $P_{uc\text{-}R}$ | Predicted ultimate axial load based on the Response Surface Method |
| $P_{ue}$ | Measured ultimate axial load |
| $V_{fs}$ | Volume fraction of steel |
| $V_{fc}$ | Volume fraction of concrete |
| $\delta_{uc\text{-}N}$ | Predicted axial shortening at ultimate load based on initial nine experiments |
| $\delta_{uc\text{-}R}$ | Predicted axial shortening at ultimate load based on the Response Surface Method |
| $\delta_{ue}$ | Measured axial shortening at ultimate point |

It was seen that for smaller $D/t$ ratio, a steel tube provides a good confinement effect for concrete [11].

O'Shea and Bridge (2000) found that the strength and ductility decrease with increasing diameter to thickness ($D/t$) ratios and confirmed from the tests that the load and the bond conditions significantly influenced the axial load behaviour [3]. Investigations from Toshiaki Fujimoto et al. (2004) noted that care appears to be necessary when using high strength concrete in combination with an ordinary strength steel tube. It is understood that the use of high strength concrete reduces the deformation capacity of concrete-filled tubes. However, the deformation capacity can be improved by using a high strength steel tube or a compact steel tube section. The ductility behavior would be improved by confining the concrete within a high strength steel tube or within a tube having a small $D/t$ ratio [12]. In the state of art report by Shanmugam and Lakshmi (2000), it was concluded that intensive research is required on the interaction between steel and concrete, the effect of concrete restraining local buckling of steel plate elements, effect of steel section, confining concrete, etc. [13].

There is a discrepancy in the analytical models proposed by different researchers for evaluating the strength of a CFT column and the effect of confinement [6]. The discrepancy was also observed while comparing predictability of different codes for CFTs under axial compression and flexure. One experimental study on circular CFTs with various concrete strengths under axial load, by Georgios Giakoumelis and Dennis Lam, observed that Eurocode 4 (EC4) provides a good prediction of the axial strength of CFT columns, 17% was the largest difference between the experimental and calculated value on the axial capacity. The predicted axial strengths using ACI (American Concrete Institute) and AS (Australian Standards) were 35% lower than the results obtained from experiments [8]. Design codes for composite steel–concrete columns such as EC4, BS (British Standards) 5950, BS 5400 and ACI-318-83 do not consider the local buckling of slender steel plates [14]. Both EC4 and AISC codes conservatively estimate the axial load capacity of slender rectangular CFT samples [15].

A series of tests were performed, by Dennis Lam and Christopher Williams,to consider the behaviour of short composite columns under axial compression. Comparisons between predictions from EC4, ACI-318 and AS with experimental results was made and it was found that ACI-318 and AS gave better prediction for axial capacity of CFTs than EC4 [16]. Experimental and theoretical studies have been carried out on behaviour of short tubular steel columns by Campione and Scibilia. The effects of different geometry and dimensions of the cross sections were investigated for a given length of the CFT and simplified expressions to predict ultimate load of short columns were proposed [17]. Previous research on slender circular composite columns shows that the strength of the column decreases as the slenderness ratio increases [18]. For thin walled composite filled columns under axial compression, strength was found to decrease with the increase of slenderness ratio and strength reduction occurred at a much higher rate for slender columns with slenderness ratio equal to or less than 24 [19]. Some studies were carried out by Manojkumar and Narasimhan (2009) on CFT beams to predict moment capacity using linear regression models based on a minimum number of experiments [20].

The present work is intended to study the parameters affecting the ultimate axial load carrying capacity and corresponding axial shortening (ductility) of the CFT using the Design Of Experiments (DOE) approach. The prime factors considered to affect ultimate axial load and corresponding axial shortening under axial compression are diameter, wall thickness of the steel tube, strength of in-fill concrete and length of the CFT. The effect of the slenderness ratio on the ultimate load carrying capacity of the CFT is considered by selecting three lengths of CFTs namely 1 m, 0.7 m and 0.5 m. The Length to diameter ratio ($L/D$) for the samples selected is 7.8–22.5 and the $D/t$ ratio is 22.3–50.8. For each length of the CFT column, 81 combinations are tested (Table 1), consisting of three diameters, three wall thicknesses and three grades of in-fill concrete ($3^3 = 27$). For each combination of CFT, three samples are tested and the average value is considered. A total of 243 experiments are conducted to determine the effect of these four factors on the responses, namely ultimate axial load ($P_{ue}$) and axial shortening at the ultimate point ($\delta_{ue}$).

## 2. Experimental programme

In the present investigation CFTs with three different diameters each with three different wall thicknesses are selected ($D/t$ = 22.3–50.58). Three different grade concrete mixes of $M_{30}$, $M_{40}$ and $M_{50}$ are considered (Table 2). Design mixes are prepared using locally available Portland Pozzolana Cement (PPC), crushed granite jelly (12.0 mm down) and river sand. The mix designs of these three grades of concrete are made based on the guidelines of IS 10262-1982 [21]. The mix proportions adopted for the three grades are shown in Table 3. In order to ensure proper compaction, a higher degree of workability i.e. 80–100 mm slump is adopted for the concrete mixes and is achieved by using silica fume and super plasticizer as admixtures. Standard cubes (100 mm size) are tested to determine the compressive strength of the concrete mixes at 28 days.

Cold-formed, mild steel tubes, with yield strength of 250 MPa and 1000 mm, 700 mm and 500 mm in length are used in the present investigation. These tubes are seam welded. The edges of the tubes are finished. The outer surface of the steel tubes are painted to avoid corrosion. The insides of the tubes are wire brushed and the deposits of grease and oil, if any, are removed. The allowable $D/t$ ratios of the steel hollow sections are less than the limits specified in EC4-1994 [22] and thus premature buckling failure of CFT specimens is avoided.

Steel tubes are kept in an upright position in a specially prepared stand, while pouring the concrete. The bottom end of the steel tube is covered tightly with polythene sheet and concrete is poured from the top. Concrete fills the steel tube in approximately four equal layers with each layer being well compacted. The top of the concrete is trimmed off using a trowel and the steel tube is kept undisturbed until it is taken out from the stand after 24 h

**Table 1**
Details of CFT samples tested for each 1 m, 0.7 m and 0.5 m length of the column.

| Sl. no. | Notation | No. of samples | Notation | No. of samples | Notation | No. of samples |
|---|---|---|---|---|---|---|
| 1 | $D_1t_1M_{30}$ | 3 | $D_2t_1M_{30}$ | 3 | $D_3t_1M_{30}$ | 3 |
| 2 | $D_1t_2M_{30}$ | 3 | $D_2t_2M_{30}$ | 3 | $D_3t_2M_{30}$ | 3 |
| 3 | $D_1t_3M_{30}$ | 3 | $D_2t_3M_{30}$ | 3 | $D_3t_3M_{30}$ | 3 |
| 4 | $D_1t_1M_{40}$ | 3 | $D_2t_1M_{40}$ | 3 | $D_3t_1M_{40}$ | 3 |
| 5 | $D_1t_2M_{40}$ | 3 | $D_2t_2M_{40}$ | 3 | $D_3t_2M_{40}$ | 3 |
| 6 | $D_1t_3M_{40}$ | 3 | $D_2t_3M_{40}$ | 3 | $D_3t_3M_{40}$ | 3 |
| 7 | $D_1t_1M_{50}$ | 3 | $D_2t_1M_{50}$ | 3 | $D_3t_1M_{50}$ | 3 |
| 8 | $D_1t_2M_{50}$ | 3 | $D_2t_2M_{50}$ | 3 | $D_3t_2M_{50}$ | 3 |
| 9 | $D_1t_3M_{50}$ | 3 | $D_2t_3M_{50}$ | 3 | $D_3t_3M_{50}$ | 3 |
| No. of samples | $D_1$ series | 27 | $D_2$ series | 27 | $D_3$ series | 27 |
| Total no. of CFT samples tested for each length | | | | | $27 + 27 + 27 = 81$ | |

Note: $M_{30}$ = Concrete Mix of characteristic strength of 30 N/mm$^2$ with cube strength at 28 days is 42.4 N/mm$^2$.
$M_{40}$ = Concrete Mix of characteristic strength of 40 N/mm$^2$ with cube strength at 28 days is 51.7 N/mm$^2$.
$M_{50}$ = Concrete Mix of characteristic strength of 50 N/mm$^2$ with cube strength at 28 days is 60.7 N/mm$^2$.

**Table 2**
Factors and levels selected for each length of the CFT column.

| Levels | Factors | | |
|---|---|---|---|
| | Diameter of the steel tube (mm) | Wall thickness of the steel tube (mm) | Strength of in-filled concrete (N/mm$^2$) |
| Level-1 | 44.45 ($D_1$) | 1.25 ($t_1$) | 42.4 ($f_{cu1}$) |
| Level-2 | 57.15 ($D_2$) | 1.6 ($t_2$) | 51.7 ($f_{cu2}$) |
| Level-3 | 63.5 ($D_3$) | 2.0 ($t_3$) | 60.7 ($f_{cu3}$) |

**Table 3**
Concrete mix proportions.

| Sl. no | Mix designation | Binder (B) (kg/Cub.m) | | Proportions B:FA:CA | $W/B$ ratio | Super plasticizer % (by wt of binder) | 28 days Compressive strength ($f_{cu}$) (N/mm$^2$) | Slump (mm) |
|---|---|---|---|---|---|---|---|---|
| | | Cement | Silica fume | | | | | |
| 1 | $M_{30}$ | 390 | 20 | 1:1.80:2.28 | 0.45 | 2.0 | 42.4 | 90 |
| 2 | $M_{40}$ | 410 | 20 | 1:1.76:2.16 | 0.40 | 2.2 | 51.7 | 80 |
| 3 | $M_{50}$ | 430 | 20 | 1:1.67:2.04 | 0.38 | 2.6 | 60.7 | 80 |

to keep in water for curing. The theoretical densities of the CFTs are computed using the law of mixtures and a comparison of these values is made with actual density of CFTs. Densities of all the CFTs are near to the theoretical densities. Such an illustration is shown in Table 4 for a typical 1 m length of samples.

## 3. Test setup and procedure

The tests are conducted on CFTs, in a 1000 kN capacity Column Testing Machine, at 28 days of age. Linearly Varying Displacement Transducers (LVDT) are placed at one fourth, mid-height and three fourths heights of the sample to measure the lateral deformation. Prior to the actual tests, a pre-load of approximately 2–5 kN is applied so that the platens of the testing machine are firmly attached to both ends of the specimen. The axial load is then applied slowly by careful manipulation of the loading-valves. The readings of the applied load, axial shortening and LVDT readings are recorded at appropriate load increments.

## 4. Results and discussion

### 4.1. Design of experimental approach

In order to save time and material cost involved in experimentation, a lesser number of experiments is desired. Therefore, the Taguchi method [23] was introduced as a useful engineering methodology to find the proper combination of structural parameters and to perform the analysis with the minimum number of experiments. Therefore nine experiments are carried out according to the combination levels indicted by an L9 orthogonal array (Table 5) for each length of the sample. An orthogonal array helps in determining the minimum number of trials that are necessary, and the factor levels for each parameter in each trial. A general L9 orthogonal array consists of three factor levels each at three levels. For each sample three replicas were tested.

### 4.2. Main effect plots and analysis of variance

After performing experiments as per Taguchi's experimental design, the main effect plots for ultimate axial load and axial shortening at ultimate load are plotted for 1 m, 0.7 m and 0.5 m length of the CFTs. The main effect is the direct effect of parameters on the response or dependent variable. Figs. 1–6 show the main effect plots of parameters with respect to the ultimate axial load and associated axial shortening for CFT columns. It is plotted by considering the means of the responses at each level of the parameters, as shown in Tables 6 and 7. From Figs. 1, 3 and 5, it can be noted that increases in diameter, wall thickness and strength of concrete will increase the ultimate axial load capacity for 1 m, 0.7 m and 0.5 m length of CFTs. However, the diameter of the steel tube has the most significant effect on both the ultimate axial load capacity and corresponding axial shortening of all the three lengths of the CFTs. The strength of the in-fill concrete and the wall thickness have respectively lesser effects compared to diameter of the steel tube. After the diameter, the wall thickness has the most influence on the ultimate axial load carrying capacity of CFTs 0.5 m in length. These CFTs act as short columns and an increase in wall thickness helps to postpone the local buckling failure. To assess the rank of each parameter, the deltas of the means of each level of all the factors are calculated and shown in Tables 6 and 7. The Delta means the value of the maximum mean minus the minimum one. The most influential factor ranks first.

**Table 4**
Theoretical and experimental density of CFTs-1 m long.

| Notation | Cross sectional area of CFT ($mm^2$) | Mass of CFT (gm) | $\rho_{exp}$ ($kN/m^3$) | $V_{fs}$ | $V_{fc}$ | $\rho_{theo}$ ($kN/m^3$) | $\rho_{exp}/\rho_{theo}$ |
|---|---|---|---|---|---|---|---|
| $D_1t_1M_{30}$ | | 4435.00 | 28.58 | 0.11 | 0.89 | 30.85 | 0.93 |
| $D_1t_2M_{30}$ | | 4783.00 | 30.82 | 0.14 | 0.86 | 32.43 | 0.95 |
| $D_1t_3M_{30}$ | | 5061.67 | 32.61 | 0.17 | 0.83 | 34.20 | 0.95 |
| $D_1t_1M_{40}$ | | 4452.67 | 28.69 | 0.11 | 0.89 | 30.85 | 0.93 |
| $D_1t_2M_{40}$ | 1551.99 | 4800.33 | 30.93 | 0.14 | 0.86 | 32.43 | 0.95 |
| $D_1t_3M_{40}$ | | 5098.00 | 32.85 | 0.17 | 0.83 | 34.20 | 0.96 |
| $D_1t_1M_{50}$ | | 4534.00 | 29.21 | 0.11 | 0.89 | 30.85 | 0.95 |
| $D_1t_2M_{50}$ | | 4815.33 | 31.03 | 0.14 | 0.86 | 32.43 | 0.96 |
| $D_1t_3M_{50}$ | | 5081.33 | 32.74 | 0.17 | 0.83 | 34.20 | 0.96 |
| $D_2t_1M_{30}$ | | 7146.00 | 27.85 | 0.09 | 0.91 | 29.58 | 0.94 |
| $D_2t_2M_{30}$ | | 7335.67 | 28.59 | 0.11 | 0.89 | 30.82 | 0.93 |
| $D_2t_3M_{30}$ | | 7816.33 | 30.47 | 0.14 | 0.86 | 32.23 | 0.95 |
| $D_2t_1M_{40}$ | | 7159.33 | 27.91 | 0.09 | 0.91 | 29.58 | 0.94 |
| $D_2t_2M_{40}$ | 2565.54 | 7519.30 | 29.31 | 0.11 | 0.89 | 30.82 | 0.95 |
| $D_2t_3M_{40}$ | | 7911.33 | 30.84 | 0.14 | 0.86 | 32.23 | 0.96 |
| $D_2t_1M_{50}$ | | 7132.67 | 27.80 | 0.09 | 0.91 | 29.58 | 0.94 |
| $D_2t_2M_{50}$ | | 7439.67 | 29.00 | 0.11 | 0.89 | 30.82 | 0.94 |
| $D_2t_3M_{50}$ | | 7983.00 | 31.12 | 0.14 | 0.86 | 32.23 | 0.97 |
| $D_3t_1M_{30}$ | | 8716.00 | 27.52 | 0.08 | 0.92 | 29.13 | 0.94 |
| $D_3t_2M_{30}$ | | 9213.33 | 29.09 | 0.10 | 0.90 | 30.26 | 0.96 |
| $D_3t_3M_{30}$ | | 9484.00 | 29.94 | 0.12 | 0.88 | 31.53 | 0.95 |
| $D_3t_1M_{40}$ | | 8786.70 | 27.74 | 0.08 | 0.92 | 29.13 | 0.95 |
| $D_3t_2M_{40}$ | 3167.33 | 9201.33 | 29.05 | 0.10 | 0.90 | 30.26 | 0.96 |
| $D_3t_3M_{40}$ | | 9581.00 | 30.25 | 0.12 | 0.88 | 31.53 | 0.96 |
| $D_3t_1M_{50}$ | | 8658.67 | 27.34 | 0.08 | 0.92 | 29.13 | 0.94 |
| $D_3t_2M_{50}$ | | 9224.00 | 29.12 | 0.10 | 0.90 | 30.26 | 0.96 |
| $D_3t_3M_{50}$ | | 9515.67 | 30.04 | 0.12 | 0.88 | 31.53 | 0.95 |

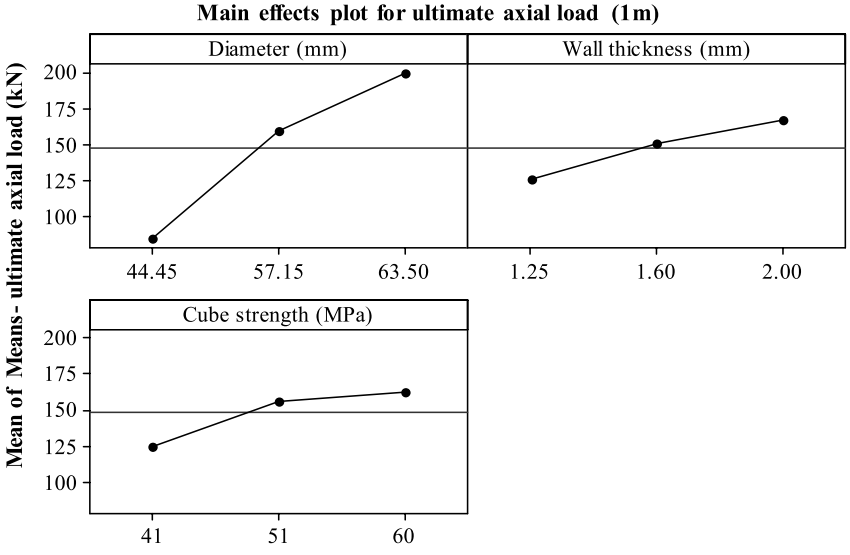


**Fig. 1.** Main effects plot for the ultimate axial load for 1 m long CFTs.

**Table 5**
L9 – Orthogonal array adopted and experimental results – for each length of CFT.

| Notation | Ultimate axial load $P_{ue}$ (kN) | | | Axial shortening at ultimate point $\delta_{ue}$ (mm) | | |
|---|---|---|---|---|---|---|
| | 1 m | 0.7 m | 0.5 m | 1 m | 0.7 m | 0.5 m |
| $D_1t_1M_{30}$ | 45.2 | 82 | 96.2 | 4.0 | 4.7 | 5.4 |
| $D_1t_2M_{40}$ | 86.5 | 117.1 | 134.1 | 4.1 | 5.0 | 5.2 |
| $D_1t_3M_{50}$ | 124 | 145.3 | 155.6 | 4.2 | 5.3 | 5.4 |
| $D_2t_1M_{40}$ | 151.6 | 176.5 | 187.5 | 6.0 | 6.3 | 5.6 |
| $D_2t_2M_{50}$ | 181.7 | 201.5 | 229 | 5.4 | 6.1 | 5.3 |
| $D_2t_3M_{30}$ | 144.3 | 205.8 | 213.7 | 8.4 | 7 | 7.3 |
| $D_3t_1M_{50}$ | 181.2 | 239.1 | 262.4 | 4.7 | 5.8 | 6.4 |
| $D_3t_2M_{30}$ | 185.6 | 226.3 | 230.5 | 7.4 | 7.6 | 7.8 |
| $D_3t_3M_{40}$ | 231.3 | 269 | 280.5 | 7.1 | 7.2 | 7.4 |

The experimental results are also analyzed using the Analysis Of Variance (ANOVA) technique. ANOVA is a statistical analysis which helps to reduce the error variance and quantifies the dominance of a control factor. This analysis aids in justifying the effects of input changes on the responses in an experiment. From ANOVA it is found that diameter of the steel tube has the most significant effect on both the ultimate axial load carrying capacity and the associated axial shortening for all the lengths of the CFTs, while the strength of the in-fill concrete and the wall thickness have respectively lesser influence on these responses. The greater **F** value confirms that the diameter of the steel tube has the most influential effect among all factors on the responses of CFTs of all the three lengths. Typical ANOVA details for CFTs of 1 m length are shown in Tables 8 and 9.

### 4.3. Verification of Taguchi's method for CFTs

After conducting the initial nine experiments, linear regression models are developed Eqs. (1)–(6) to predict ultimate axial load

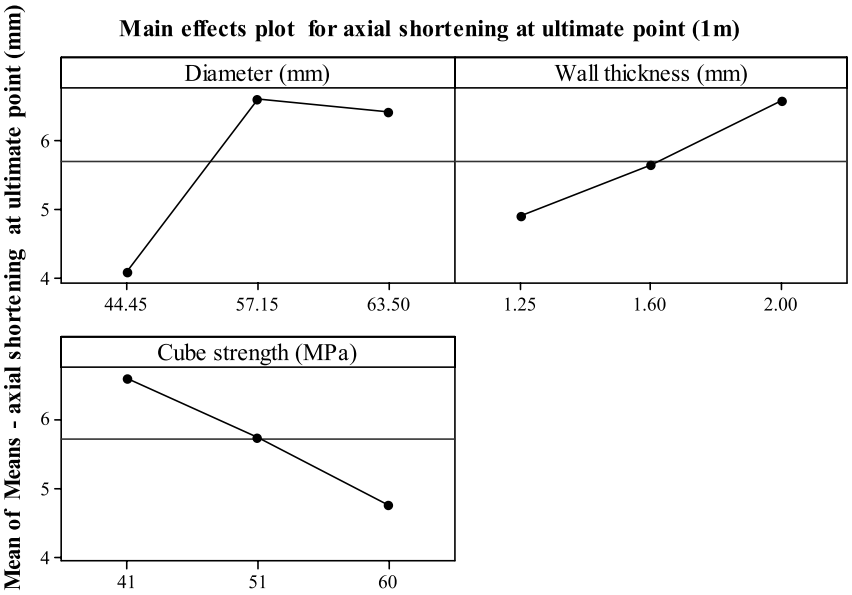


**Fig. 2.** Main effects plot for axial shortening at the ultimate load for 1m long CFTs.

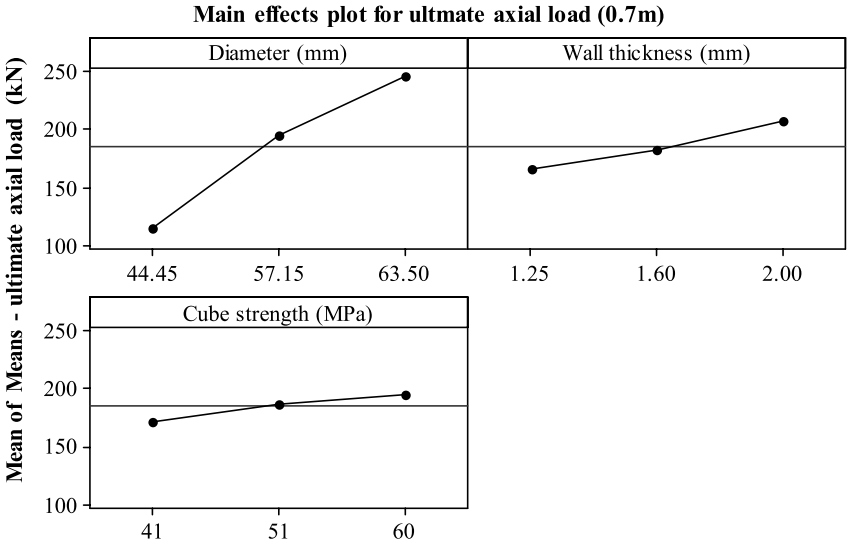


**Fig. 3.** Main effects plot for the ultimate axial load for 0.7 m long CFTs.

and axial shortening at the ultimate point for each length of the CFT samples.

*CFTs*—1 m *long*

$$P_{uc\text{-}N} = -368 + 5.97D + 53.7t + 1.98f_{cu} \quad (1)$$

$$\delta_{uc\text{-}N} = -0.26 + 0.132D + 2.22t - 0.0963f_{cu}. \quad (2)$$

*CFTs*—0.7 m *long*

$$P_{uc\text{-}N} = -339 + 6.75D + 54.6t + 1.27f_{cu} \quad (3)$$

$$\delta_{uc\text{-}N} = 0.52 + 0.100D + 1.19t - 0.0367f_{cu}. \quad (4)$$

*CFTs*—0.5 m *long*

$$P_{uc\text{-}N} = -341 + 6.73D + 46.1t + 1.87f_{cu} \quad (5)$$

$$\delta_{uc\text{-}N} = 2.21 + 0.0922D + 1.21t - 0.0600f_{cu}. \quad (6)$$

$P_{uc\text{-}N}$ = Predicted ultimate axial load based on initial nine experiments (kN)

$\delta_{uc\text{-}N}$ = Predicted axial shortening at ultimate load based on initial nine experiments (mm)

$D$ = Outer diameter of the steel tube (mm)

$t$ = Wall thickness of the steel tube (mm)

$f_{cu}$ = Cube compressive strength of concrete at 28 days (MPa)

These models are used to predict the axial load carrying capacity and associated axial shortening at the ultimate point of all the other CFT samples used in the experimental programme. To verify the accuracy of such predictions of the load carrying capacity and corresponding axial shortening, actual axial compression tests are now conducted for remaining samples, and a comparison of experimental values is made with the predicted values. It is observed that the regression models based on nine experiments predict the ultimate axial load carrying capacity very well, and reasonably well for axial shortening at ultimate point, for all the three lengths of the CFTs. A plot of experimental values vs predicted ($P_{uc\text{-}N}$ vs $P_{ue}$ and $\delta_{uc\text{-}N}$ vs $\delta_{ue}$) values for each 1 m, 0.7 m and 0.5 m length of the CFTs are shown in Figs. 7–9.

Experimental investigations were carried out by Gupta et al. [11] on circular concrete filled steel tubes subjected to axial compression. The steel tubes used in their study were of diameter 47.28 mm–112.56 mm and the lengths of the CFT were 340 mm.

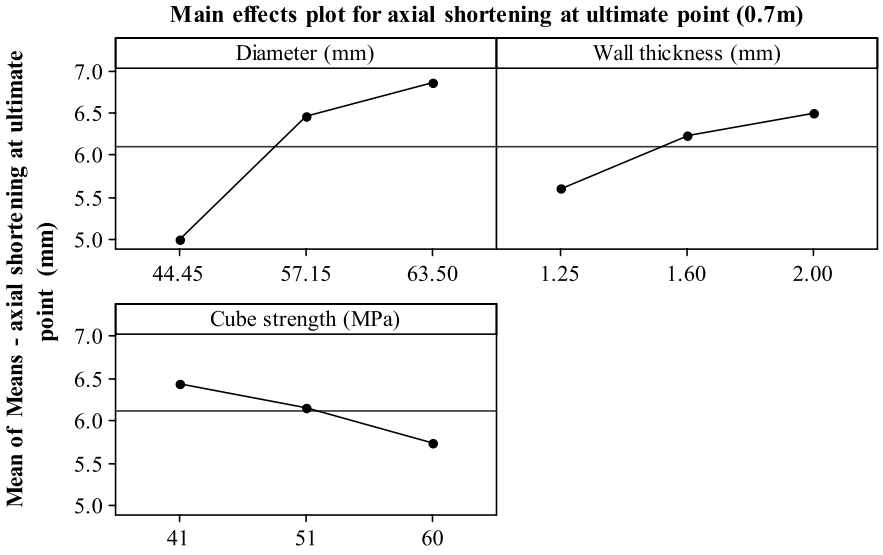


**Fig. 4.** Main effects plot for axial shortening at the ultimate load for 0.7 m long CFTs.

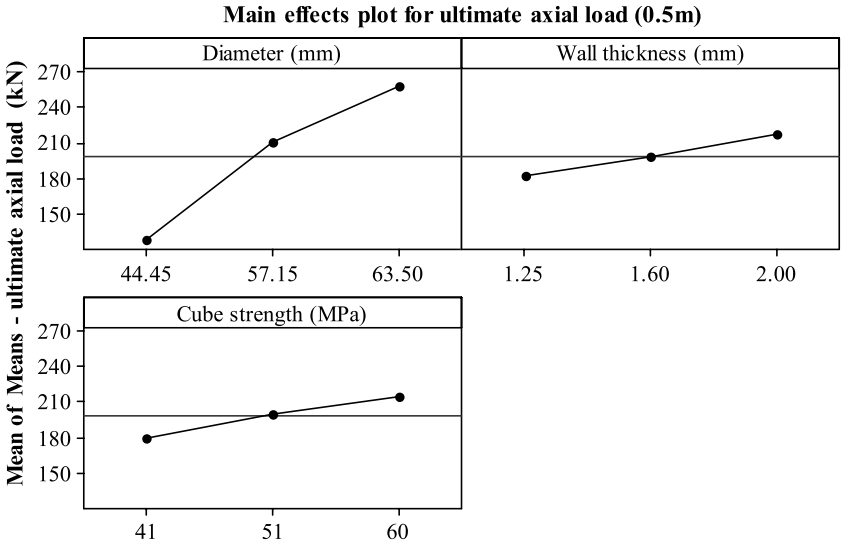


**Fig. 5.** Main effects plot for the ultimate axial load for 0.5 m long CFTs.

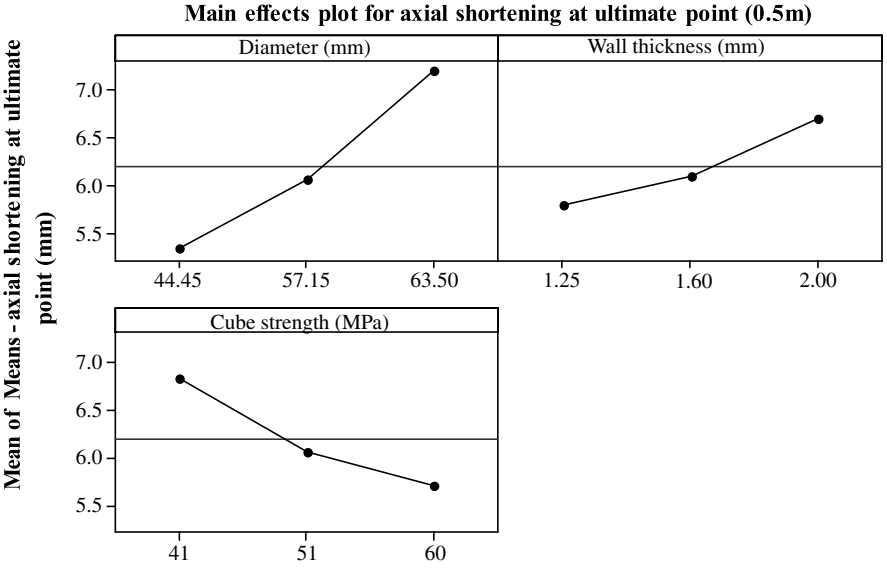


**Fig. 6.** Main effects plot for axial shortening at the ultimate load for 0.5 m long CFTs.

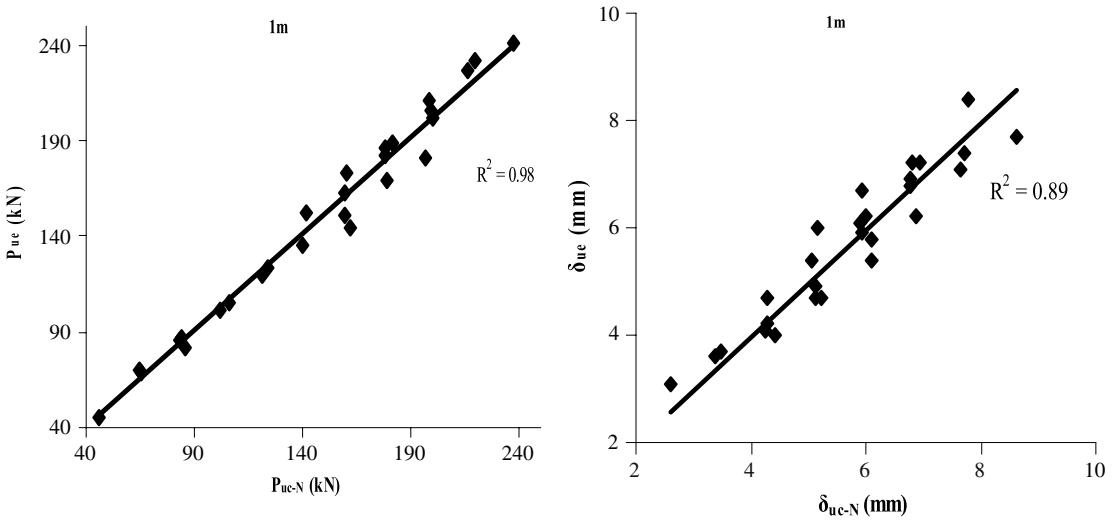


**Fig. 7.** Predicted values of axial load and axial shortening at the ultimate point vs experimental results — Linear regression analysis (1 m).

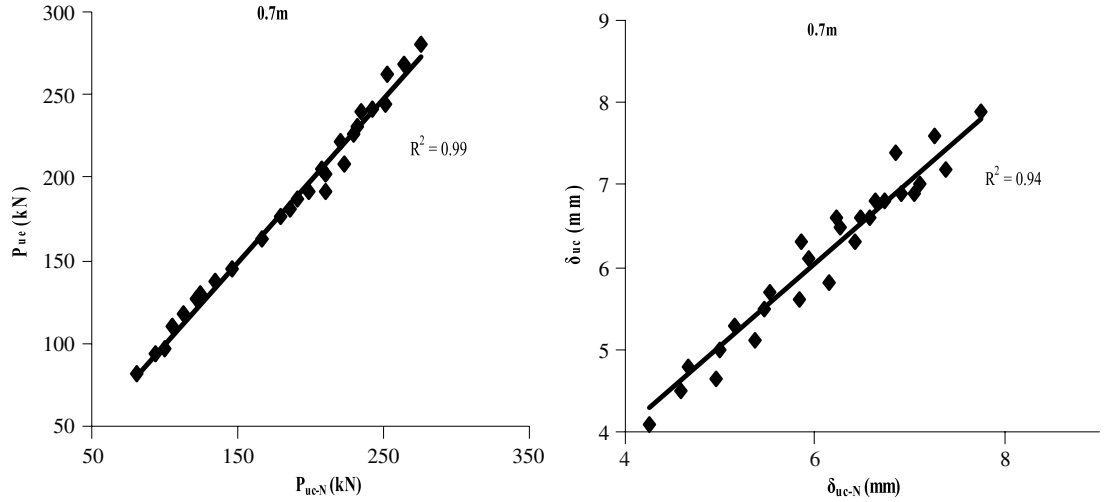


**Fig. 8.** Predicted values of axial load and axial shortening at the ultimate point vs experimental results — Linear regression analysis (0.7 m).

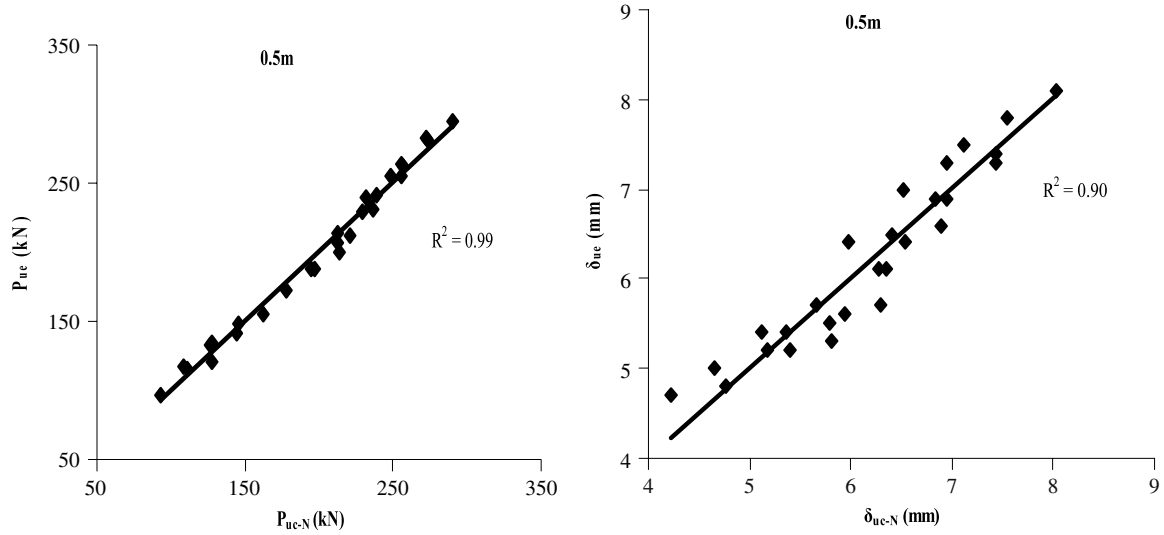


**Fig. 9.** Predicted values of axial load and axial shortening at the ultimate point vs experimental results — Linear regression analysis (0.5 m).

Tests were performed using $M_{30}$ and $M_{40}$ grade concrete as infill for the steel tubes and the load carrying capacities of those CFTs were in the range of 156 kN–770 kN. The test results of $M_{30}$ grade concrete of Gupta et al. [11] are combined with the test

**Table 6**
Response table for means of mean values of each level — ultimate axial load.

| Level | Length of the CFT—1.0 m | | | Length of the CFT—0.7 m | | | Length of the CFT—0.5 m | | |
|---|---|---|---|---|---|---|---|---|---|
| | $D$ (mm) | $t$ (mm) | $f_{cu}$ (N/mm$^2$) | $D$ (mm) | $t$ (mm) | $f_{cu}$ (N/mm$^2$) | $D$ (mm) | $t$ (mm) | $f_{cu}$ (N/mm$^2$) |
| 1 | 85.23 | 126.00 | 125.03 | 114.80 | 165.90 | 171.40 | 128.60 | 182.00 | 180.10 |
| 2 | 159.20 | 151.27 | 156.47 | 194.60 | 181.60 | 187.5 | 210.1 | 197.90 | 200.70 |
| 3 | 199.37 | 166.53 | 162.30 | 244.80 | 206.70 | 195.3 | 257.80 | 216.60 | 215.70 |
| Delta | 114.13 | 40.53 | 37.27 | 130.00 | 40.80 | 23.9 | 129.2 | 34.6 | 35.5 |
| Rank | 1 | 2 | 3 | 1 | 2 | 3 | 1 | 3 | 2 |

**Table 7**
Response table for means of mean values of each level of three factors — axial shortening at ultimate point.

| Level | Length of the CFT—1.0 m | | | Length of the CFT—0.7 m | | | Length of the CFT—0.5 m | | |
|---|---|---|---|---|---|---|---|---|---|
| | $D$ (mm) | $t$ (mm) | $f_{cu}$ (N/mm$^2$) | $D$ (mm) | $t$ (mm) | $f_{cu}$ (N/mm$^2$) | $D$ (mm) | $t$ (mm) | $f_{cu}$ (N/mm$^2$) |
| 1 | 4.10 | 4.90 | 6.60 | 5.00 | 5.60 | 6.43 | 5.33 | 5.80 | 6.83 |
| 2 | 6.60 | 5.63 | 5.73 | 6.46 | 6.23 | 6.16 | 6.06 | 6.10 | 6.06 |
| 3 | 6.40 | 6.56 | 4.76 | 6.86 | 6.50 | 5.73 | 7.20 | 6.70 | 5.70 |
| Delta | 2.50 | 1.66 | 1.83 | 1.86 | 0.90 | 0.70 | 1.86 | 0.90 | 1.13 |
| Rank | 1 | 3 | 2 | 1 | 2 | 3 | 1 | 3 | 2 |

**Table 8**
ANOVA table for the response – ultimate axial load – 1 m.

| Source | DF | Sum of squares | Adj MS | **F** |
|---|---|---|---|---|
| Diameter | 2 | 20 110.8 | 10 055.4 | **39.66** |
| Thickness | 2 | 2 514.4 | 1 257.2 | **4.96** |
| Cube strength of the concrete | 2 | 2 410.9 | 1 205.4 | **4.75** |
| Error | 2 | 507.1 | 253.6 | |
| Total | 8 | 25 543.3 | | |

**Table 9**
ANOVA table for the response – axial shortening at ultimate point – 1 m.

| Source | DF | Sum of squares | Adj MS | **F** |
|---|---|---|---|---|
| Diameter | 2 | 11.5800 | 5.7900 | **56.03** |
| Thickness | 2 | 4.1867 | 2.0933 | **20.26** |
| Cube strength of the concrete | 2 | 5.0467 | 2.5233 | **24.42** |
| Error | 2 | 0.2067 | 0.1033 | |
| Total | 8 | 21.0200 | | |

results of the present experimental investigations and a simple linear regression model is developed (Eq. (7)) to generalize the model for CFTs of diameter 44.45 mm–112.56 mm. To validate the model further, part of the experimental test results of Gupta et al. are used and the axial compressive strengths of CFTs with $M_{40}$ grade concrete were predicted using Eq. (7). It is found that the regression model so developed predicts the ultimate axial load carrying capacity of the CFTs very well. A plot of experimental values vs predicted values based on Eq. (7) is shown in Fig. 10.

$$P_{uc\text{-}G} = -176 + 6.88D + 73.0t + 1.93f_{cu} - 0.437L \quad (7)$$

$P_{uc\text{-}G}$ = Generalized regression model to predict the ultimate axial load (kN) for short columns.

### 4.4. Interaction models

Based on the test results of these twenty seven experiments performed for each length of the CFTs, regression models are also developed (Eqs. (8)–(13)) using the Response Surface Method (RSM), to account for the interaction between the test variables on the ultimate axial load carrying capacity and the corresponding axial shortening.

*CFTs*—1 m *long*

$$P_{uc\text{-}R} = -512.84 + 5.007D + 97.365t + 7.38f_{cu} - 0.010D^2 - 42.741t^2 - 0.065{f_{cu}}^2 + 1.169D.t + 0.005D.f_{cu} + 0.691t.f_{cu} \quad (8)$$

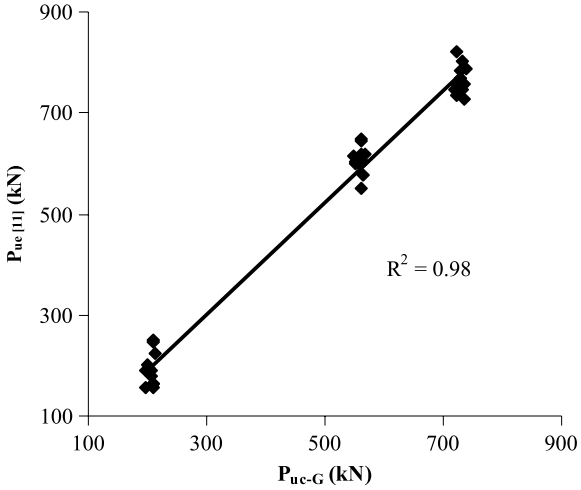


**Fig. 10.** Predicted values of ultimate axial load using the generalized regression model vs experimental results [11].

$$\delta_{uc\text{-}R} = -26.915 + 0.744D + 1.958t + 0.321f_{cu} - 0.0051D^2 - 0.0053t^2 - 0.0031{f_{cu}}^2 + 0.0019D.t - 0.0014D.f_{cu} - 0.0047t.f_{cu}. \quad (9)$$

*CFTs*—0.7 m *long*

$$P_{uc\text{-}R} = -155.326 + 0.162D + 61.844t + 0.455f_{cu} + 0.036D^2 - 3.974t^2 + 0.002{f_{cu}}^2 + 0.623D.t + 0.030D.f_{cu} - 0.440t.f_{cu} \quad (10)$$

$$\delta_{uc\text{-}R} = -12.676 + 0.449D + 2.540t + 0.077f_{cu} - 0.0018D^2 - 0.4180t^2 - 0.0004f_{cu}^2 - 0.0261D.t - 0.0021D.f_{cu} + 0.0249t.f_{cu}. \quad (11)$$

*CFTs*—0.5 m *long*

$$P_{uc\text{-}R} = -88.651 - 3.606D + 61.844t + 0.455f_{cu} + 0.036D^2 - 3.974t^2 + 0.002{f_{cu}}^2 + 0.623D.t + 0.030D.f_{cu} - 0.440t.f_{cu} \quad (12)$$

$$\delta_{uc\text{-}R} = -12.676 + 0.449D + 2.540t + 0.077f_{cu} - 0.0018D^2 - 0.4180t^2 - 0.0004{f_{cu}}^2 - 0.0261D.t - 0.0021D.f_{cu} + 0.0249t.f_{cu} \quad (13)$$

$P_{uc\text{-}R}$ = Predicted ultimate axial load based on the Response Surface Method (kN)

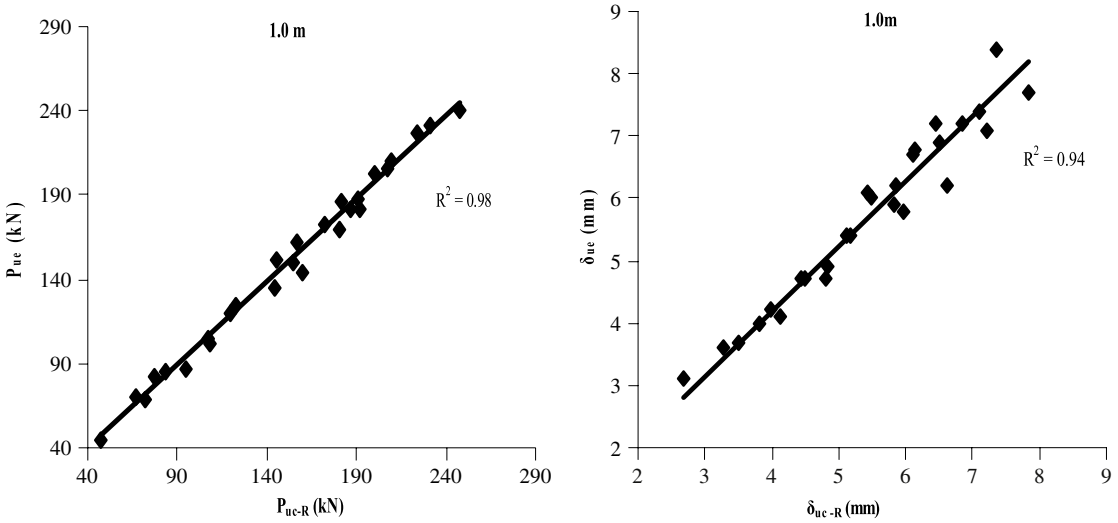


**Fig. 11.** Predicted values of axial load and axial shortening at the ultimate point vs experimental results — Regression analysis based on the RSM (1.0 m).

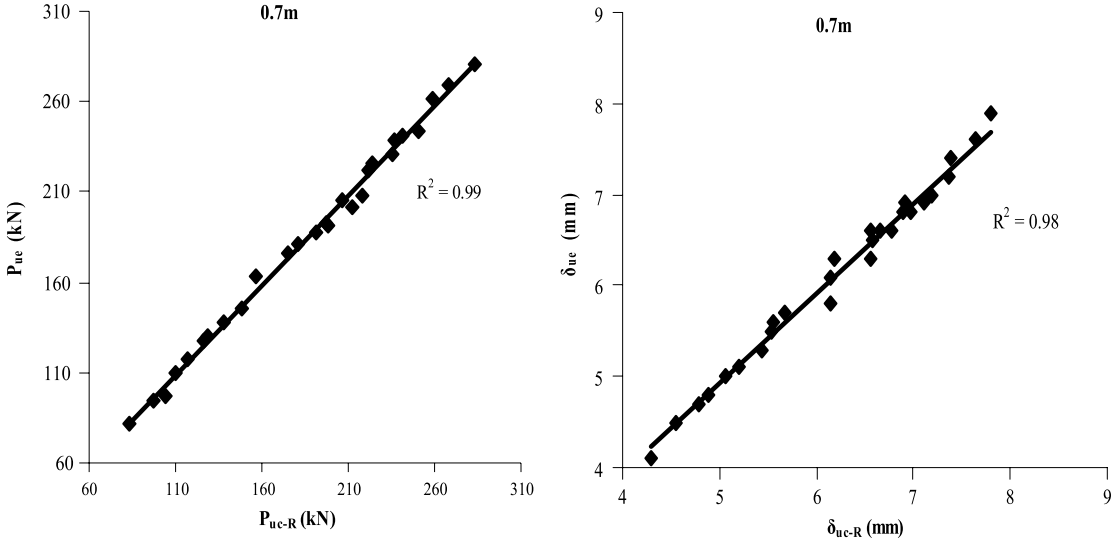


**Fig. 12.** Predicted values of axial load and axial shortening at the ultimate point vs experimental results — Regression analysis based on the RSM (0.7 m).

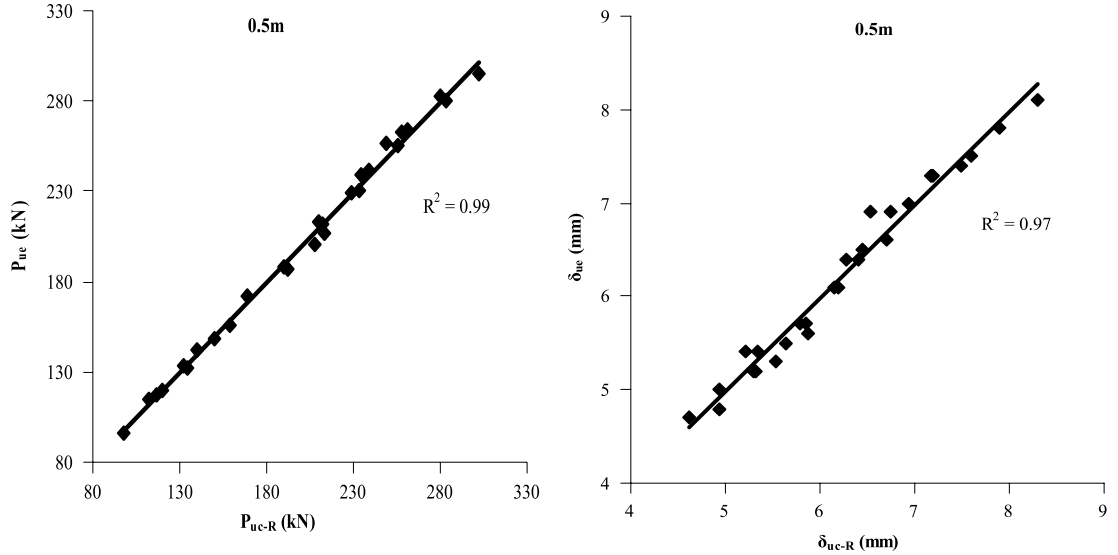


**Fig. 13.** Predicted values of axial load and axial shortening at the ultimate point vs experimental results — Regression analysis based on the RSM (0.5 m).

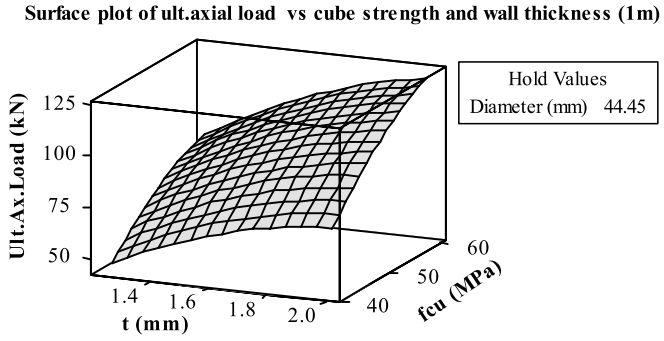


**Fig. 14.** Surface plot of axial load at the ultimate point vs cube strength and wall thickness for CFTs — 1 m long.

$\delta_{uc\text{-}R}$ = Predicted axial shortening at the ultimate load based on the Response Surface Method (mm)

Using these regression models, the ultimate axial load and corresponding axial shortening of CFTs are predicted. A plot of actual experimental values vs predicted values for each 1 m, 0.7 m and 0.5 m length of the CFTs are shown in Figs. 11–13. It is found that, for all the three lengths of the CFTs, these interactions are more accurate for the prediction of ultimate axial load than for the axial shortening at the ultimate point.

### 4.5. Interaction plots

Typical response surface plots and contour plots for the ultimate axial load for both 1 m and 0.7 m lengths of the CFTs have been drawn using MINITAB (version 14). The response surface plots indicate the effect of any two variables together on the axial load capacity at the ultimate point. A typical response surface plot shown in Fig. 14 explains the effect of wall thickness and cube strength of in-fill concrete together on the axial load capacity at the ultimate point. Contour plots are useful to arrive at the proper combination of tube diameter, wall thickness and cube strength of

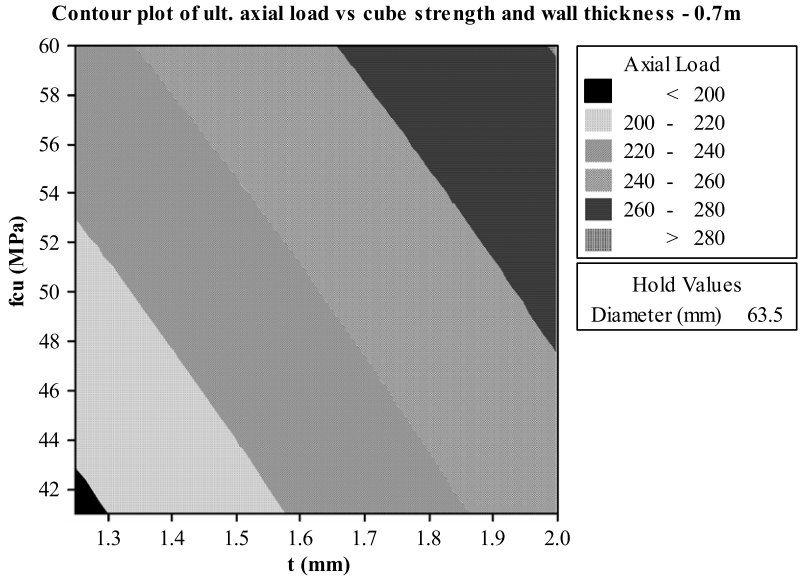


**Fig. 15.** Contour plot of axial load at the ultimate point vs. cube strength and wall thickness for CFTs — 0.7 m long.

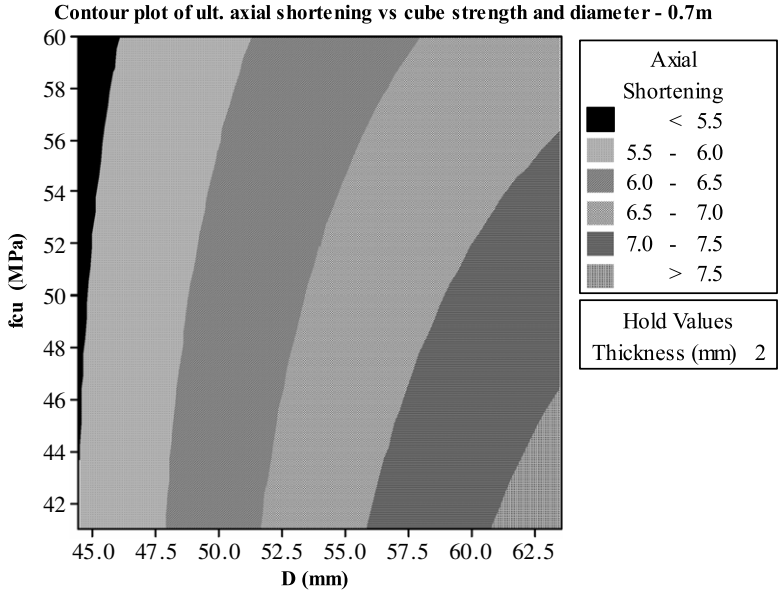


**Fig. 16.** Contour plot of axial shortening at the ultimate point vs cube strength and diameter for CFTs — 0.7 m long.

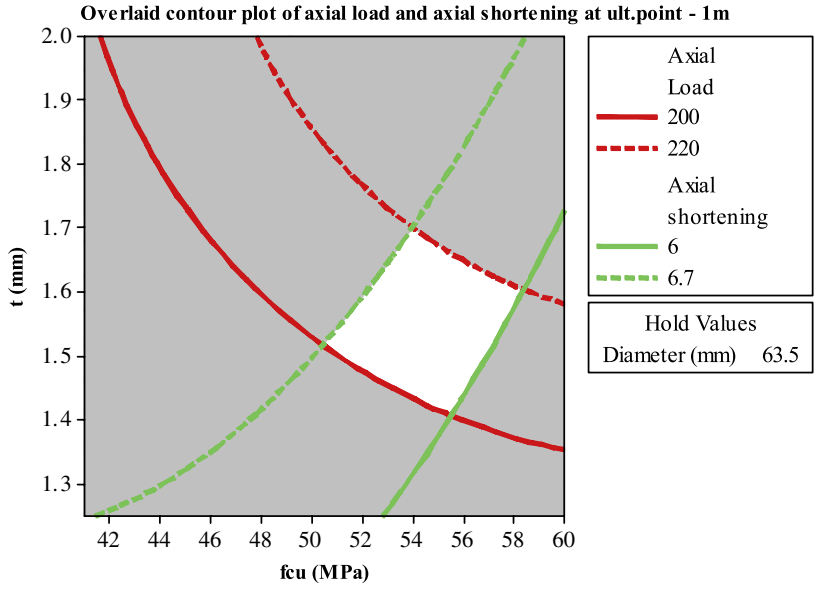


**Fig. 17.** Overlaid contour plot of axial load and axial shortening at the ultimate point for CFTs — 1.0 m long ($D = 63.5$ mm).

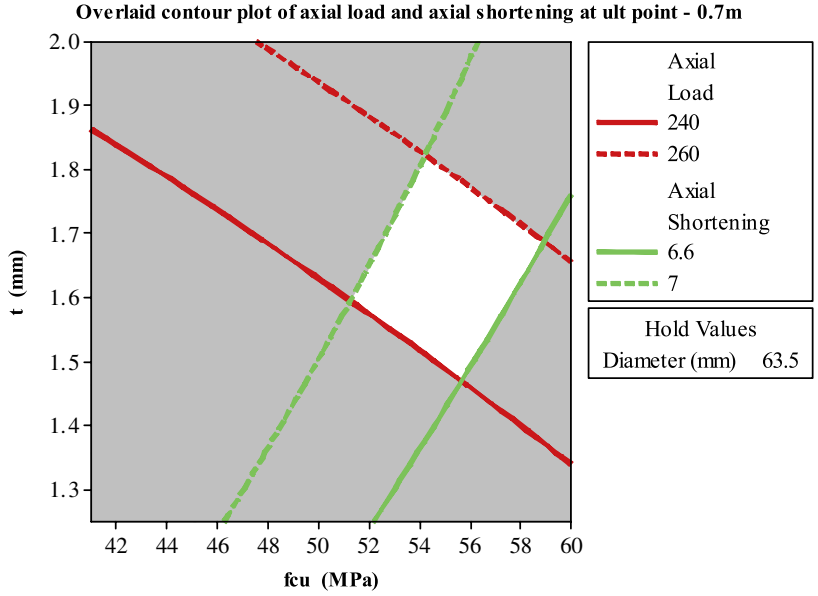


**Fig. 18.** Overlaid contour plot of axial load and axial shortening at the ultimate point for CFTs — 0.7 m long ($D = 63.5$ mm).

in-fill concrete for given values of axial load or axial shortening at the ultimate point of the CFTs. Typical contour plots for axial load and axial shortening of 0.7 m long CFTs are shown in Fig. 15 and Fig. 16 respectively. The overlaid contour plots are useful to choose a combination of any two of the variables amongst diameter, wall thickness and cube strength of in-fill concrete for a certain range of design axial load capacity and the corresponding axial shortening. A set of overlaid contour plots shown in Figs. 17–19. Fig. 17 demonstrates the combination of cube strength of in-fill concrete and wall thickness for the axial load capacity in the range 200–220 kN and the corresponding axial shortening in the range 6.0–6.7 mm for the CFT of 1 m long and 63.5 mm diameter. Similarly Figs. 18 and 19 shows the combination of cube strength of in-fill concrete and wall thickness for the axial load capacity in the range 240–260 kN and the corresponding axial shortening in the range 6.6–7.0 mm and 7.0–7.5 mm for the CFTs of 0.7m and 0.5 m length, respectively.

### *4.6. Comparison of experimental results with EC4 and AISC-LRFD specifications*

The results obtained in the present experimental work were compared with the predictions based on EC4-1994 [22] and AISC-LRFD-2005 [24] code provisions. EC4 uses the limit state concept to achieve the aims of serviceability and safety, by applying a partial safety factor to the load and material properties. When calculating predicted values from the codes, all the partial safety factors are taken as unity. Comparisons of the experimental ultimate load of test specimens with predictions based on code provisions for three lengths of CFTs are shown in Tables 10 and 11. When the relative slenderness $\bar{\lambda}$ (as defined in Equation 6.39 of EC4-1994) is greater than 0.5 the confinement effect is minimum. However, the composite action can be improved to some extent by choosing an appropriate combination of the strength of steel and the strength of concrete. Here an attempt is made to study the effect of changing $\bar{\lambda}$ on the axial load capacities of short and long columns (Table 11).

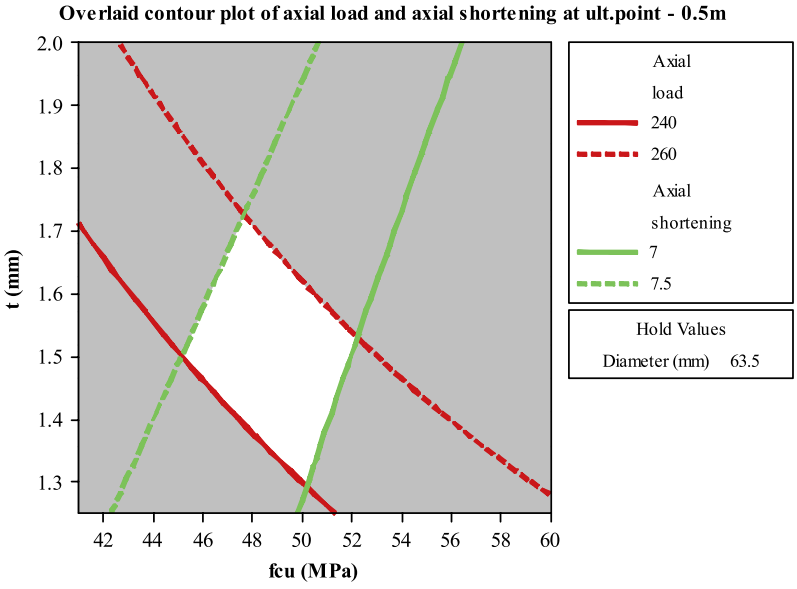


**Fig. 19.** Overlaid contour plot of axial load and axial shortening at the ultimate point for CFTs — 0.5 m long ($D = 63.5$ mm).

**Table 10**
Comparison of experimental results with AISC Codes.

| Notation | 1 m | | | 0.7 m | | | 0.5 m | | |
|---|---|---|---|---|---|---|---|---|---|
| | $P_{ue}$ (kN) | $P_{AISC}$ (kN) | $P_{ue}/P_{AISC}$ | $P_{ue}$ (kN) | $P_{AISC}$ (kN) | $P_{ue}/P_{AISC}$ | $P_{ue}$ (kN) | $P_{AISC}$ (kN) | $P_{ue}/P_{AISC}$ |
| $D_1t_1M_{30}$ | 45.20 | 79.78 | 0.57 | 82.00 | 82.51 | 0.99 | 96.20 | 83.83 | 1.15 |
| $D_1t_2M_{30}$ | 69.40 | 88.34 | 0.79 | 96.50 | 91.79 | 1.05 | 117.20 | 93.47 | 1.25 |
| $D_1t_3M_{30}$ | 82.00 | 97.71 | 0.84 | 127.10 | 102.09 | 1.24 | 132.70 | 104.22 | 1.27 |
| $D_1t_1M_{40}$ | 68.60 | 90.49 | 0.76 | 94.00 | 93.66 | 1.00 | 114.70 | 95.19 | 1.20 |
| $D_1t_2M_{40}$ | 86.50 | 98.64 | 0.88 | 117.10 | 102.55 | 1.14 | 134.10 | 104.45 | 1.28 |
| $D_1t_3M_{40}$ | 104.80 | 107.58 | 0.97 | 138.00 | 112.42 | 1.23 | 148.40 | 114.77 | 1.29 |
| $D_1t_1M_{50}$ | 85.40 | 101.10 | 0.84 | 109.90 | 104.76 | 1.05 | 120.30 | 106.52 | 1.13 |
| $D_1t_2M_{50}$ | 101.00 | 108.85 | 0.93 | 130.00 | 113.25 | 1.15 | 141.70 | 115.38 | 1.23 |
| $D_1t_3M_{50}$ | 124.00 | 117.34 | 1.06 | 145.30 | 122.68 | 1.18 | 155.60 | 125.27 | 1.24 |
| $D_2t_1M_{30}$ | 119.80 | 123.07 | 0.97 | 163.00 | 125.33 | 1.30 | 171.70 | 126.40 | 1.36 |
| $D_2t_2M_{30}$ | 135.00 | 135.12 | 1.00 | 181.60 | 137.89 | 1.32 | 188.50 | 139.22 | 1.35 |
| $D_2t_3M_{30}$ | 144.30 | 148.54 | 0.97 | 205.80 | 151.98 | 1.35 | 213.70 | 153.62 | 1.39 |
| $D_1t_1M_{40}$ | 151.60 | 141.88 | 1.07 | 176.50 | 144.57 | 1.22 | 187.50 | 145.86 | 1.29 |
| $D_2t_2M_{40}$ | 173.10 | 153.40 | 1.13 | 192.10 | 156.63 | 1.23 | 206.30 | 158.17 | 1.30 |
| $D_2t_3M_{40}$ | 188.30 | 166.24 | 1.13 | 221.90 | 170.14 | 1.30 | 239.30 | 172.00 | 1.39 |
| $D_2t_1M_{50}$ | 162.00 | 160.58 | 1.01 | 187.20 | 163.75 | 1.14 | 200.30 | 165.26 | 1.21 |
| $D_2t_2M_{50}$ | 181.70 | 171.57 | 1.06 | 201.50 | 175.29 | 1.15 | 229.00 | 177.06 | 1.29 |
| $D_2t_3M_{50}$ | 206.10 | 183.82 | 1.12 | 231.30 | 188.22 | 1.23 | 256.00 | 190.33 | 1.35 |
| $D_3t_1M_{30}$ | 150.50 | 146.86 | 1.02 | 191.30 | 149.27 | 1.28 | 211.70 | 150.42 | 1.41 |
| $D_3t_2M_{30}$ | 185.60 | 161.16 | 1.15 | 226.30 | 163.73 | 1.38 | 230.50 | 164.95 | 1.40 |
| $D_3t_3M_{30}$ | 202.30 | 177.23 | 1.14 | 243.60 | 180.01 | 1.35 | 255.00 | 181.34 | 1.41 |
| $D_3t_1M_{40}$ | 169.30 | 170.37 | 0.99 | 208.00 | 173.29 | 1.20 | 241.60 | 174.69 | 1.38 |
| $D_3t_2M_{40}$ | 210.50 | 184.22 | 1.14 | 240.80 | 187.25 | 1.29 | 264.10 | 188.69 | 1.40 |
| $D_3t_3M_{40}$ | 231.30 | 199.76 | 1.16 | 269.00 | 202.95 | 1.33 | 280.50 | 204.46 | 1.37 |
| $D_3t_1M_{50}$ | 181.20 | 193.75 | 0.94 | 239.10 | 197.22 | 1.21 | 262.40 | 198.88 | 1.32 |
| $D_3t_2M_{50}$ | 226.70 | 207.16 | 1.09 | 262.00 | 210.68 | 1.24 | 283.00 | 212.35 | 1.33 |
| $D_3t_3M_{50}$ | 240.60 | 222.17 | 1.08 | 280.20 | 225.80 | 1.24 | 294.60 | 227.53 | 1.29 |

The comparison of results indicates that the predicted ultimate load carrying capacity for 1 m long CFTs from both the codes is much higher compared to the experimental values. However, for 0.5 m and 0.7 m long CFTs the predictions of ultimate load by the codes are fairly good.

## 5. Conclusions

Results of experimental investigations on circular CFT samples with $D/t$ ratio of 22.3–50.8 and $L/D$ ratio of 7.8–22.5 have been presented in this paper. From the experimental results, the following broad conclusions can be drawn.

1. Regression models developed with a minimum number of experiments based on the Taguchi method predict the axial load carrying capacity very well and the axial shortening at the ultimate point reasonably well.
2. The diameter of the steel tube has the most significant effect on both the ultimate axial load and the corresponding axial shortening of the CFTs.
3. Regression models developed using the Response Surface Method for the ultimate axial load and the corresponding axial shortening account for the interaction between the test variables.
4. The larger variation for slender CFTs between the experimental values and the values predicted from the codes indicates that more studies are needed and the codal provisions should be refined.

**Table 11**
Comparison of experimental axial load capacities with those predicted by EC4 for change in $\bar{\lambda}$.

| Notation | $\bar{\lambda}$ | | | $P_{EC4}$ (kN) | | | $P_{ue}/P_{EC4}$ | | |
|---|---|---|---|---|---|---|---|---|---|
| | 1 m | 0.7 m | 0.5 m | 1 m | 0.7 m | 0.5 m | 1 m | 0.7 m | 0.5 m |
| $D_1t_1M_{30}$ | 0.89 | 0.62 | 0.45 | 92.78 | 92.78 | 92.78 | 0.49 | 0.88 | 1.04 |
| $D_1t_2M_{30}$ | 0.88 | 0.61 | 0.44 | 102.55 | 102.55 | 103.25 | 0.68 | 0.94 | 1.14 |
| $D_1t_3M_{30}$ | 0.86 | 0.60 | 0.43 | 113.51 | 113.51 | 114.68 | 0.72 | 1.12 | 1.16 |
| $D_1t_1M_{40}$ | 0.95 | 0.66 | 0.50 | 106.40 | 106.40 | 106.40 | 0.64 | 0.88 | 1.08 |
| $D_1t_2M_{40}$ | 0.92 | 0.65 | 0.48 | 115.72 | 115.72 | 115.72 | 0.75 | 1.01 | 1.16 |
| $D_1t_3M_{40}$ | 0.91 | 0.63 | 0.47 | 126.18 | 126.18 | 126.18 | 0.83 | 1.09 | 1.18 |
| $D_1t_1M_{50}$ | 1.00 | 0.70 | 0.52 | 120.03 | 120.03 | 120.03 | 0.71 | 0.92 | 1.00 |
| $D_1t_2M_{50}$ | 0.97 | 0.68 | 0.50 | 128.90 | 128.90 | 128.90 | 0.78 | 1.01 | 1.10 |
| $D_1t_3M_{50}$ | 0.95 | 0.66 | 0.49 | 138.86 | 138.86 | 138.86 | 0.89 | 1.05 | 1.12 |
| $D_2t_1M_{30}$ | 0.71 | 0.50 | 0.35 | 140.35 | 140.35 | 146.53 | 0.85 | 1.16 | 1.17 |
| $D_2t_2M_{30}$ | 0.69 | 0.49 | 0.35 | 153.10 | 153.10 | 161.55 | 0.88 | 1.19 | 1.17 |
| $D_2t_3M_{30}$ | 0.68 | 0.48 | 0.34 | 167.48 | 167.48 | 178.47 | 0.86 | 1.23 | 1.20 |
| $D_2t_1M_{40}$ | 0.76 | 0.53 | 0.40 | 163.48 | 163.48 | 163.55 | 0.93 | 1.08 | 1.15 |
| $D_2t_2M_{40}$ | 0.74 | 0.52 | 0.39 | 175.65 | 175.65 | 176.33 | 0.99 | 1.09 | 1.17 |
| $D_2t_3M_{40}$ | 0.72 | 0.50 | 0.37 | 189.36 | 189.36 | 190.82 | 0.99 | 1.17 | 1.25 |
| $D_2t_1M_{50}$ | 0.80 | 0.56 | 0.42 | 186.61 | 186.61 | 185.96 | 0.87 | 1.00 | 1.08 |
| $D_2t_2M_{50}$ | 0.78 | 0.54 | 0.41 | 198.19 | 198.19 | 197.90 | 0.92 | 1.02 | 1.16 |
| $D_2t_3M_{50}$ | 0.76 | 0.53 | 0.39 | 211.24 | 211.24 | 211.51 | 0.98 | 1.09 | 1.21 |
| $D_3t_1M_{30}$ | 0.64 | 0.45 | 0.32 | 167.60 | 167.60 | 177.82 | 0.90 | 1.14 | 1.19 |
| $D_3t_2M_{30}$ | 0.63 | 0.44 | 0.31 | 181.85 | 181.85 | 195.52 | 1.02 | 1.24 | 1.18 |
| $D_3t_3M_{30}$ | 0.62 | 0.43 | 0.31 | 197.92 | 199.58 | 215.50 | 1.02 | 1.22 | 1.18 |
| $D_3t_1M_{40}$ | 0.69 | 0.48 | 0.37 | 196.42 | 196.42 | 198.18 | 0.86 | 1.06 | 1.22 |
| $D_3t_2M_{40}$ | 0.67 | 0.47 | 0.35 | 210.01 | 210.01 | 213.08 | 1.00 | 1.15 | 1.24 |
| $D_3t_3M_{40}$ | 0.66 | 0.46 | 0.34 | 225.34 | 225.34 | 230.01 | 1.03 | 1.19 | 1.22 |
| $D_3t_1M_{50}$ | 0.73 | 0.51 | 0.39 | 225.24 | 225.24 | 225.84 | 0.80 | 1.06 | 1.16 |
| $D_3t_2M_{50}$ | 0.71 | 0.50 | 0.37 | 238.17 | 238.17 | 239.77 | 0.95 | 1.10 | 1.18 |
| $D_3t_3M_{50}$ | 0.69 | 0.48 | 0.36 | 252.76 | 252.76 | 255.69 | 0.95 | 1.11 | 1.15 |

## Acknowledgements

The authors are grateful to M/s Shankara Pipes Private Limited, Bangalore, India for providing all the steel tubes used in the experimental programme.

## References

[1] Zhong Tao, Han Lin-Hai, Wang Dong-Ye. Strength and ductility of stiffened thin-walled hollow steel structural stub columns filled with concrete. Thin-Walled Structures 2008;46:1113–28.
[2] Han LH. Tests on stub columns of concrete-filled RHS sections. Journal of Constructional Steel Research 2002;58(3):353–72.
[3] O'Shea MD, Bridge RQ. Design of circular thin-walled concrete filled steel tubes. Journal of Structural Engineering, ASCE 2000;126(11):1295–303.
[4] Zeghiche J, Chaoui K. An experimental behaviour of concrete-filled steel tubular column. Journal of Constructional Steel Research 2005;61:53–66.
[5] Gourley Brett C, Tort Cenk, Hajjar Jerome F, Schiller Paul H. A synopsis of studies of the monotonic and cyclic behavior of concrete filled steel tube beam-columns structural engineering report No. ST-01-4. Version 3.0; 2001.
[6] Elremaily Ahmed, Azizinamini Atorod. Behavior and strength of circular concrete-filled tube columns. Journal of Constructional Steel Research 2002; 58:1567–91.
[7] Schinder Stephen P. Axially loaded concrete filled steel tubes. Journal of Structural Engineering ASCE 1998;124(10):1125–38.
[8] Giakoumelis Georgios, Lam Dennis. Axial capacity of circular concrete-filled tube columns. Journal of Constructional Steel Research 2004;60:1049–68.
[9] Sakino Kenji, Nakahara Hiroyuki, Morino Shosuke, Nishiyama Isao. Behavior of centrally loaded concrete-filled steel-tube short columns. Journal of Structural Engineering, ASCE 2004;130(2):180–8.
[10] Oyawaa Walter O, Sugiurab Kunitomo, Watanabe Eiichi. Polymer concrete-filled steel tubes under axial compression. Construction and Building Materials 2001;15:187–97.
[11] Gupta PK, Sarda SM, Kumar MS. Experimental and computational study of concrete filled steel tubular columns under axial loads. Journal of Constructional Steel Research 2007;63:182–93.
[12] Fujimoto Toshiaki, Mukai Akiyoshi, Nishiyama Isao, Sakino Kenji. Behavior of eccentrically loaded concrete-filled steel tubular columns. Journal of Structural Engineering 2004;130(2):203–12.
[13] Shanmugam NE, Lakshmi B. State of the art report on steel–concrete composite columns. Journal of Constructional Steel Research 2001;57:1041–80.
[14] Shanmugam NE, Lakshmi B, Uy B. An analytical model for thin-walled steel box columns with concrete in-fill. Engineering Structures 2002;24:825–38.
[15] Chitawadagi Manojkumar V, Narasimhan Mattur C, Kulkarni SM. Axial capacity of rectangular concrete-filled steel tube columns — DOE approach. Construction and Building Materials 2010;24:585–95.
[16] Lam Dennis, Williams Christopher A. Experimental study on concrete filled square hollow sections. Steel and Composite Structures 2004;4(2).
[17] Campione G, Scibilia N. Beam-column behavior of concrete filled steel tubes. Steel and Composite Structures 2002;2(4).
[18] Ramana Gopal S, Devadas Manoharan P. Experimental behaviour of eccentrically loaded slender circular hollow steel columns. Journal of Constructional Steel Research 2006;62:513–20.
[19] Anwar Hossain Khandaker M. Axial load behavior of thin walled composite columns. Composites: Part B 2003;34:715–25.
[20] Chitawadagi Manojkumar V, Narasimhan Mattur C. Strength deformation behaviour of circular concrete filled steel tubes subjected to pure bending. Journal of Constructional Steel Research 2009;65:1836–45.
[21] IS 10262-1982. Indian standard recommended guidelines for concrete mix design. Bureau of Indian Standards, New Delhi, India.
[22] Eurocode 4. Design of composite steel and concrete structures, part 1.1: General rules and rules for buildings. European Committee for Standardization. EN 1994-1-1; 2004.
[23] Montgomery Douglas. Design and analysis of experiments. 5th ed. NewYork: John Wiley & Sons (ASIA) Pvt. Ltd; 2004.
[24] American Institute of Steel Construction (AISC). Manual for Structural Steel Buildings: Load and Resistance Factor Design (LRFD), Chicago; 2005.